Influence of polishing length on the sensitivity of D-shaped fiber-based refractive index sensor for alcohol detection

FARRA IZZANY TARMIZI[1], NIK NOOR HARYATUL ELEENA NIK MAHMUD[1], SITI NOOR HAMIZAH ADAM[1], WAN MARYAM WAN AHMAD KAMIL[1], SITI KHADIJAH MOHD BAKHORI[1], AHMAD RAZIF MUHAMMAD[2], SULAIMAN WADI HARUN[3], AFIQ ARIF AMINUDDIN JAFRY[1,*]
[1]*School of Physics, Universiti Sains Malaysia, 11800 USM, Penang, Malaysia*
[2]*Institute of Microengineering and Nanoelectronics (IMEN), Universiti Kebangsaan Malaysia (UKM), Bangi 43600, Selangor, Malaysia*
[3]*Photonics Engineering Laboratory, Department of Electrical Engineering, Faculty of Engineering, University of Malaya, 50603 Kuala Lumpur, Malaysia*

This study investigates the influence of polishing lengths on the sensitivity of the D-shaped fiber (DSF)-based refractive index sensor. The DSF was prepared using the polishing wheel technique, utilizing polishing bits with diameters of 1, 2, 3, and 4 mm. The DSF sensors were coated with zinc oxide-polyvinyl alcohol, which acts as a light-matter interaction enhancer for refractive index detection. The probe detects isopropyl alcohol with a concentration ranging from 0 to 100%. The result shows the sensor's sensitivity reached a maximum of 0.1942 nm/RIU and a resolution of 2.05×10^{-2} RIU within the refractive index range of 1.33-1.38, demonstrating the effectiveness of the DSF probe. All DSF-coated with ZnO probes have a high linearity of above 95%. In contrast, the uncoated DSF exhibits a lower linearity (80%), indicating that ZnO is an excellent coating material for RI sensing. Additionally, the analysis reveals a direct correlation between the polishing length and the sensor's performance, underscoring the potential for optimizing the polishing process to improve sensitivity. The findings suggest that DSF sensors are promising candidates for high-precision refractive index detection in various applications.

(Received August 5, 2025; accepted April 8, 2026)

Keywords: D-shaped fiber, Refractive index sensor, Zinc oxide, Biosensor

1. Introduction

The refractive index (RI) sensor is an important tool in detecting the RI of the surrounding medium, indicating the presence and concentration of certain substances [1]. Traditional optical fibers have been widely used in these sensors due to their high sensitivity and versatility. A fiber-based sensing probe has obtained 1200 nm/RIU sensitivity when detecting RI ranging from 1.33 to 1.38 using a single-mode fiber-based Mach-Zender interferometer [2]. Other studies achieved a sensitivity of 3000 nm/RIU in the RI ranging from 1.45 to 1.55 by using hollow-core optical fibers [3]. The results show excellent RI detection with potential applications in pharmacology, medicine, and the food industry. However, the evolution of D-shaped fiber (DSF) which involves creating a flat surface by polishing a portion of the fiber has opened a new avenue for enhancing sensor performance. The flat surface of the DSF allows better interaction between the evanescent field of the guided light and the surrounding medium, leading to improved sensitivity [4]. A DSF coated with gold film achieved a sensitivity of 4200 nm/RIU in the range of 1.33-1.40 [5]. A high-sensitivity sensing probe was due to the strong evanescent field interaction between gold and the polished surface of DSF.

Zinc oxide (ZnO) is a semiconductor material known for its magnificent optical and electronic properties. ZnO has a wide bandgap of 3.2-3.4 eV at room temperature, it also exhibits a strong absorption in the ultraviolet region ($\lambda < 400$ nm) [6, 7]. On the other hand, ZnO shows minimal absorption in the near-infrared (NIR) region. However, its electronic structure can be modified by doping with different transition metals such as cobalt, which will introduce mid-gap states that enable absorption in both visible and NIR region [8]. The electron mobility of ZnO varies significantly based on the crystal quality, doping, and measurement conditions. For undoped ZnO, the electron mobility ranges from 200-500 cm^2/Vs [9]. Due to its high electron mobility, wide bandgap, and good transparency, ZnO is a great candidate to coat optical fiber [10]. The high refractive index and wide bandgap of ZnO can enhance the interaction between the guided light and the surrounding medium, thus increasing the sensor's sensitivity [11]. In addition, the chemical stability and biocompatibility of ZnO make it suitable for a wide range of sensing application [12]. Recent studies show that the electron mobility of ZnO depends on the doping elements where ZnMgO/ZnO heterostructures exhibit electron mobility of 5500 cm^2/Vs at very low temperature [13].

Several techniques have been demonstrated to produce a sensing probe based on ZnO-coated DSF for RI

sensing. For instance, a DSF sensor based on Au/ZnO has achieved a maximum sensitivity of 15,433 nm/RIU within a RI detection range of 1.29-1.42 [14]. Other than that, Au-ZnO coated photonic crystal fiber (PCF) shows a good detection capability within the RI of 1.40-1.48, this probe is useful to detect chemical, analytes, and oil samples [15]. Another research demonstrates graphene and ZnO-coated D-shaped PCF with a 50 nm depth removed exhibits a sensitivity of 22 100 nm/RIU within the RI detection range of 1.38-1.42 [16]. Most studies focused on optimizing the coating thickness, deposition method, or type of fibers. Only a few studies investigate how the depth of the polished region influences the sensor's sensitivity and accuracy. For example, a gold-coated DSF sensor with different polishing depths achieved a maximum sensitivity of 3317.14 nm/RIU in the range of 1.34–1.40 [17]. Hence, we proposed a ZnO-DSF sensing probe with different polishing lengths. The length of the polished region may directly affect the interaction between the evanescent field and ZnO coating.

This research aims to enhance the sensitivity and accuracy of refractive index sensing by investigating the effect of DSF polishing length on the sensing probe sensitivity. We fabricate the DSF using the mechanical wheel technique. This method allows precise control over the polishing lengths of DSF to evaluate its impact on the sensor's performance. The DSF geometrical structure will be examined under the microscope to confirm its polishing length. Then, ZnO will be deposited onto the surface of the DSF structure. We confirmed the probes' elemental constituents and surface topography using field emission scanning electron microscopy (FESEM) and energy dispersive X-ray spectroscopy (EDX). The optimized ZnO-coated DSF sensor will be evaluated by immersing the sensor in alcohol and measuring the wavelength shifts on the optical spectrum analyzer. This study aims to design a high-performance ZnO-coated DSF sensor that provides an understanding of the fundamental parameters of a DSF-based sensor probe toward a highly efficient RI sensor.

2. Sensing principle and the fabrication of ZnO-coated D-shaped Fiber

The light that propagates along the core of DSF is related to the cutoff penetration depth (h_c), which is critical to determine the probe's sensitivity. The following formulas governed the evanescent wave mechanism:

$$\theta_{lm} = \sin^{-1}(\beta_{lm}/kn_1) \quad (1)$$

$$a_{eff} = a + x_s(\theta_{lm}) \quad (2)$$

where the meridional angle of incidence (θ_{lm}) and effective mode radius (a_{eff}) for each azimuthal order (l), and mode of radial order (m) can be calculated based on the propagation constant of lm mode (β_{lm}), wavenumber (k), and the enlargement caused by Goos-Hänchen shift (x_s). Assume that $n_1 \approx n_2$, x_s for transverse electric (TE) and magnetic (TM) is said to be the same. Therefore, the enlargement can now be calculated from the following expression:

$$x_s = 1/\left[k(n_1^2 sin^2\theta_{lm} - n_2^2)^{1/2}\right] \quad (3)$$

In the case that the diameter of the polished region is the same as the effective mode radius, the reflection angle can be assumed to be $\theta_{lm} - \emptyset_t$, with $\emptyset_t$ as the angle between the tangential plane to the polished region and the angle between the z-axes. The angle of incidence becomes $\theta_{lm} - 2\emptyset_t$, referring to the normal of the interface, making the ray extend to the core interface. Therefore, the angle of incidence moves closer to the critical angle due to the modification of the cladding thickness. The cutoff angle can now be calculated based on the following equation:

$$\emptyset_c = \frac{\theta_{lm} - \theta_{cr}}{2} \quad (4)$$

where θ_{cr} is the critical angle of the frustrated total internal reflection (TIR), and the cutoff penetrating depth can be calculated based on the following equation:

$$h_c = \frac{D}{2} - a_{eff} + R(1 - \cos\emptyset_c) \quad (5)$$

where D is the fiber diameter, and R is the radius of the polisher. Therefore, it is important to investigate DSF parameters, such as polishing length and depth, to evaluate the probe's sensitivity.

A workstation was set up by assembling the DREMEL 200 rotary tool to its base, as shown in Fig. 1 (a). First, the tube was attached to the base, and the base was flipped as the hex bolt and square nut were attached. The square nut was inserted into the drill press, and the height adjustment lever was lightly screwed on. The cap was removed from the tube, and the inner tube was slightly pushed out. By twisting in opposite directions, the tube was locked in place. The tube assembly was then slid into the drill press. The height-adjustment lever was adjusted, and the tube was secured to the base. Subsequently, the workstation was mounted to the optical table with screws to secure it. The nose cap was removed from the rotary tool, and the diamond polishing bit was installed. Finally, the rotary tool was inserted into the drill press. To secure the tool in place, the clamp nut was tightened.

The initial step in fabricating the SMF-28 fiber involved stripping the fiber. The process began by cutting the jacket and coating using a fiber optic stripper. To ensure the absence of buffer or any impurities, the fiber was cleaned with 99% isopropyl alcohol (IPA). Then, the fiber was placed onto the stage of the fiber cleaver and clamped to prevent movement. The fiber was then cleaved at a 90° angle to obtain a smooth surface for optimal splicing. The fiber was cleaned again with IPA to remove any remaining impurities that might affect the splicing process. After that, both fibers were placed on the stage of the fusion splicer machine. The splicing process was monitored through the screen of the splicer for any uneven surfaces of the fiber. The next step was the polishing of the fiber. The fiber was clamped using fiber holders to ensure that the tension along the fiber was evenly distributed; this also avoids any misalignment or damage that could affect the polishing process. The center of the fiber was placed over the diamond bit. One end of the fiber was connected

to a white light source while the other was connected to an optical power meter to monitor the progress of the polishing process. The fiber was polished with an insertion loss of 4 dB and monitored using the optical power meter. The polishing bits used were 1-, 2-, 3-, and 4-mm. Fig. 1 (c-d) shows the microscopic image and graphs of the D-shaped fiber prepared using different polishing bits.

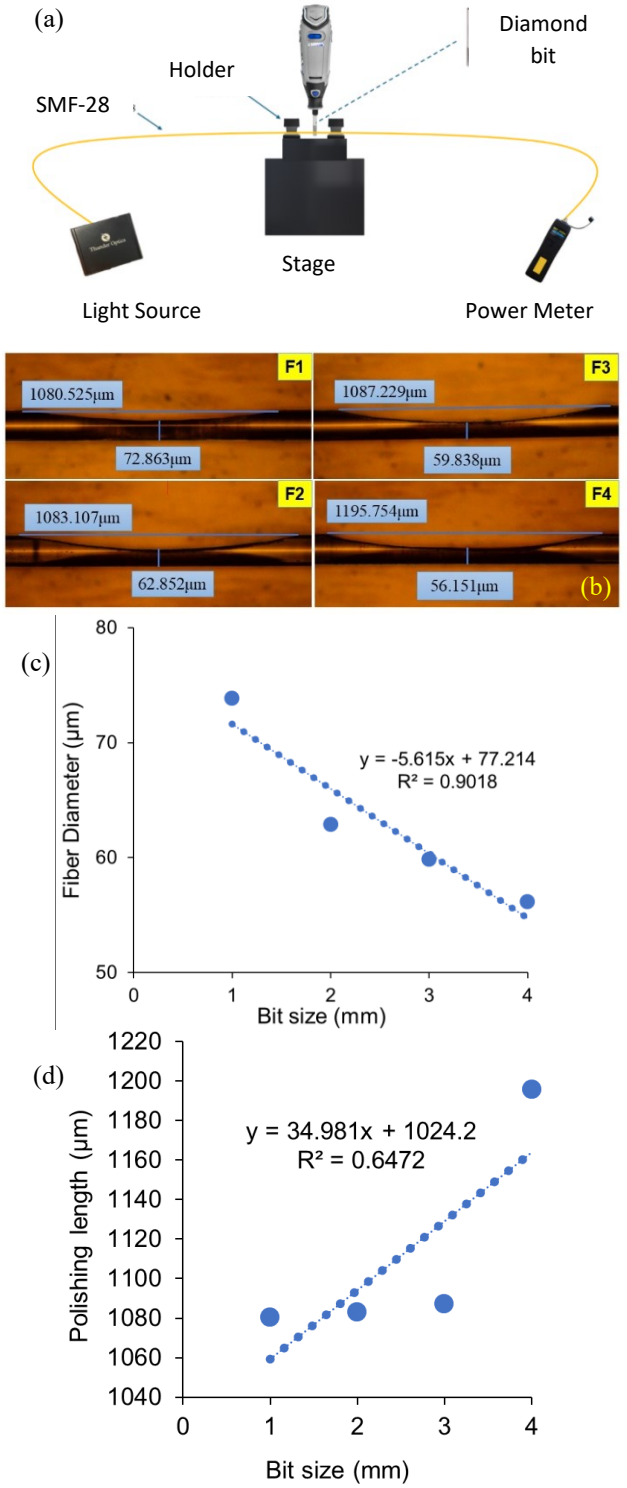

Fig. 1. Preparation and characterization of D-shaped fiber sensing probe. (a) Schematic diagram of polishing wheel technique, (b) Microscopic images of F1, F2, F3, and F4, (c) graph of remaining fiber diameter against bit size, and (d) graph of polishing length against bit size (colour online)

The length of the polished region was then measured under the microscope, and the microscopic images obtained are shown in Fig. 1 (b). The polishing lengths obtained for 1, 2, 3, and 4 mm are 1080.525, 1083.107, 1087.229, and 1195.754 µm, respectively. The remaining fiber diameters obtained for 1, 2, 3, and 4 mm are 72.863, 62.852, 59.838, and 56.151 µm, respectively. For reference, DSF polished with a 1 mm bit was marked as Fiber 1 (F1), a 2 mm bit as Fiber 2 (F2), a 3 mm bit as Fiber 3 (F3), and a 4 mm bit as Fiber 4 (F4). Referring to Fig. 1 (c), the remaining fiber diameter decreases as the bit size increases. A lower remaining fiber diameter indicates a more penetrating depth of the DSF structure. Based on the data, it is logical to assume that a polisher with a bigger radius can remove more cladding than one with a smaller radius. In contrast, the polishing length increases as the bit size increases, as shown in Fig. 1 (d). The larger bit size removes more surface, and it causes a deeper and longer polishing region on the DSF surface. Based on Fig. 1(d), the polishing length does not increase linearly with bit size. This is due to multiple factors, including uneven pressure distribution and different polishing times. This will affect the polishing process, which occurs at a faster or slower rate.

The solution of ZnO-polyvinyl alcohol (PVA) was prepared by mixing ZnO powder and PVA powder. 1 g of PVA was poured part by part into the 25 ml of deionized water. This step was crucial as it prevents the mixture from coagulating. The mixture was stirred on a hot plate for 6 hours at 70-80 °C. Then, 0.6 g of ZnO was slowly poured into the beaker. The mixture was stirred for another 2 hours. The mixture was sonicated for 1 hour to ensure it dissolved completely. A drop of ZnO-PVA solution was applied onto the surface of DSF while connecting one end to the laser source and the other to an optical power meter.

The surface topography and composition of the ZnO were examined using FESEM. The quality of the zinc oxide coating and its uniformity were visualized using the high-resolution images obtained from FESEM. Fig. 2 (a) shows the FESEM image of the ZnO-PVA coating on the DSF sample. The image was obtained using 50,000x magnification and 1 µm resolution. A red circle in the image shows a nanorod-like shape of the ZnO. However, ZnO with a more uniform interface can be obtained by synthesizing the coating material using complicated setups such as molecular beam epitaxy, sputtering, and spin coating. It proves a successful synthesis of ZnO-PVA through a simple stirring and sonication method. The presence of zinc oxide composition on the DSF structure was observed using EDX. In Fig. 2 (b), the atomic percent of Zn and O obtained are 45.34 % and 54.66 %, respectively. The weight percent obtained for Zn and O are 77.22 % and 22.78 %, respectively.

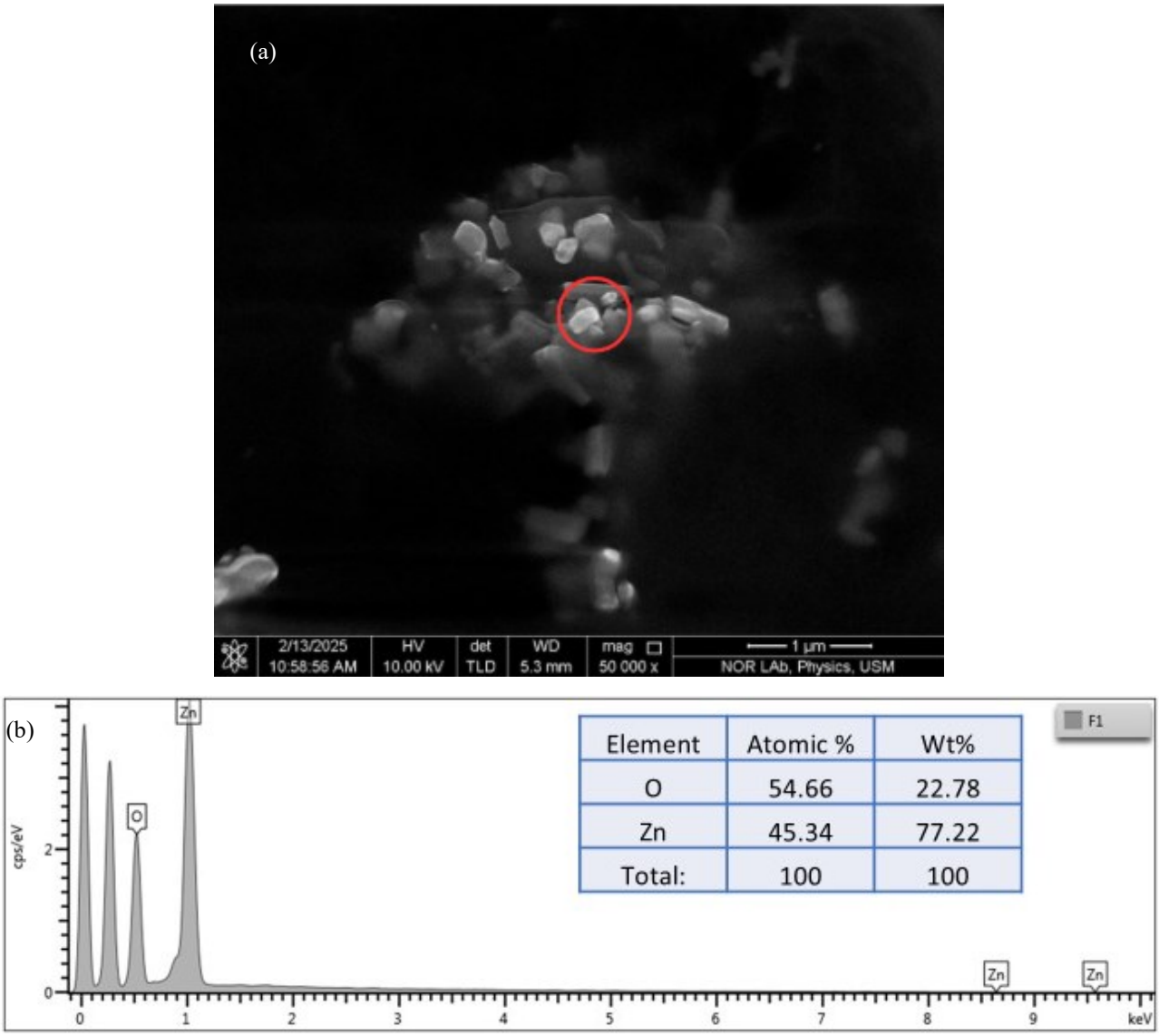

Fig. 2. Characterization of ZnO-PVA-coated D-shaped Fiber. (a) FESEM image, and (b) EDX spectrum

3. Experimental configuration

IPA solution of different concentrations was prepared by mixing IPA with deionized water. The concentration of the IPA solution was varied by a 20% increment, which was 20, 40, 60, 80, and 100%. A 1550 nm laser was used as a light source and connected to the ZnO-PVA-coated DSF as a sensing probe. A tuneable ITU-grid DFB laser (OptiSci ED-WDM series educator kit) was utilized as a laser source, with tuning ranges of 1548.4-1550.8 nm. The other ends of the sensor probe were connected to a 50/50 coupler that splits the light equally to an optical spectrum analyzer (OSA) and optical power meter (OPM) for monitoring purposes. The experimental setup for sensitivity measurement of the sensing probe is depicted in Fig. 3. Then, the ZnO-PVA-coated DSF was immersed in the 20% IPA in a petri dish. The experiment was repeated several times to ensure the repeatability and consistency of the fiber sensor. Then, the IPA solution was changed to 40%, 60%, 80%, and 100% to analyze the power and wavelength shifts of the sensing probes.

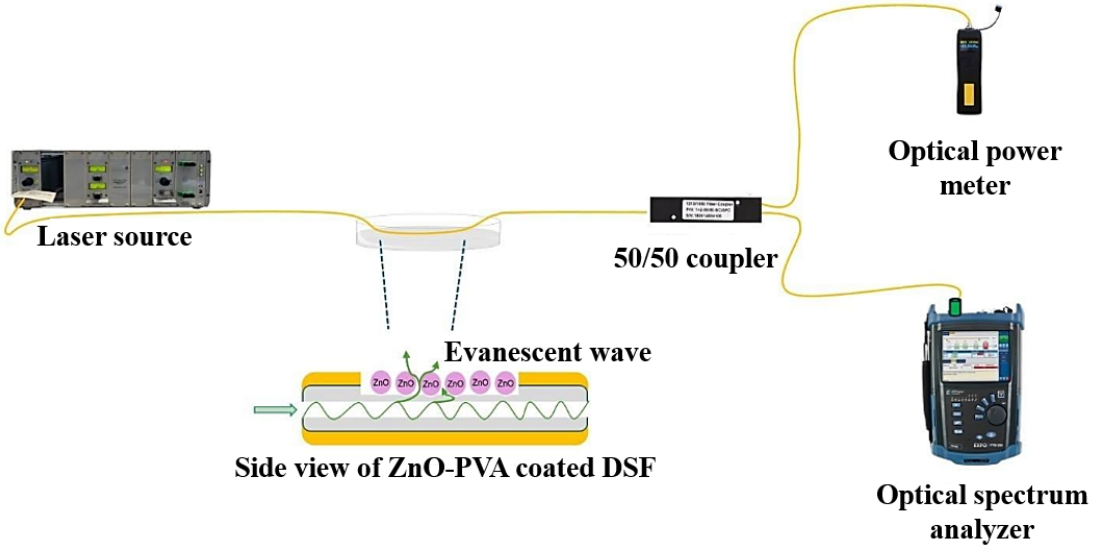

Fig. 3. Experimental setup of ZnO-PVA-coated DSF as a sensing probe for IPA solution (colour online)

4. Results and discussion

Fig. 4 shows an increasing trend between the refractive index and IPA concentration, indicating that the RI increases linearly with the increase in IPA concentration. The graph in Fig. 4 has a linearity of 0.9057, showing a consistent measurement of RI using the refractometer. Higher concentrations of IPA demonstrate that there are more particles in the solution, which slows down the speed of light and increases the RI. When the concentration increases, the interaction between molecules changes, which causes an increase in overall density and leads to an increase in RI. The slope of the graph is 0.0005 RIU/%. The IPA concentration of 20 to 100 % owns RI values of 1.33 to 1.38 RIU. The fitting line has a linearity of 90.57 %, indicating a reliable trend of RI changes against concentrations. This trend also shows precise control over the preparation procedure of IPA analytes for RI detection, which contributes to a reliable sensing measurement.

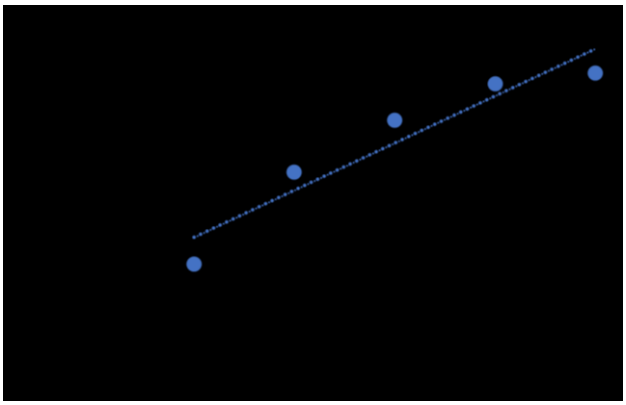

Fig. 4. The refractive index of isopropyl alcohol solution against its concentration

Fig. 5 (a-d) shows the shifting of the peak wavelength of transmitted light with FI, F2, F3, and F4 as sensing probes. All graphs show the redshifted peak wavelength, indicating reliable sensing probes with all 4 fibers. The inset of each graph indicates a wavelength shift to the right side of the spectrum with increasing concentration. The ZnO-PVA coating that interacts with the IPA molecules leads to higher absorbance, which causes a redshifted wavelength of the sensing probe. As depicted in Fig. 5 (c), F3 has a wider tuning range of 0.01 nm within the wavelength range from 1550.006 to 1550.016 nm, compared to the other 3 fibers. This allows the sensing probe to detect a broader measurement range and more detectable resonance shifts that improve sensing sensitivity. The tuning ranges for F1, F2, and F4 are 0.007, 0.005, and 0.008 nm, respectively.

Fig. 6 shows an increasing graph of peak wavelength versus refractive index. This indicates that as the RI of the IPA solution increases, the wavelength of the transmitted light shifts towards longer wavelengths. Table 1 shows the sensing parameters of all four DSF probes, including sensing sensitivity, resolution, and linearity. Fiber 3 has the highest sensitivity of 0.1942 nm/RIU, compared to fibers 1, 2, and 4. The resolution was calculated based on the standard deviation of each probe's wavelength shift. Fiber 3 also has the smallest resolution of 2.05×10^{-2} RIU. This indicates the ability of fiber 3 to detect small changes in RI for precise monitoring of physical and chemical changes. On the other hand, fibers 1, 2, and 4 own resolutions of 2.10×10^{-2}, 2.22×10^{-2}, and 3.36×10^{-2} RIU, respectively. In addition, fibers 2, 3, and 4 own nearly similar linearities of 0.97, indicating the probes' ability to detect consistent RI changes in alcohol solution. Whereas fiber 1 has the lowest linearity of 0.95, a low linearity shows inconsistency of RI sensing using this probe. All sensor probes (F1-F4) exhibit tunability of output power between 0 and 0.4 dB; all 4 probes show similar intensity tunability, indicating a reliable sensing setup.

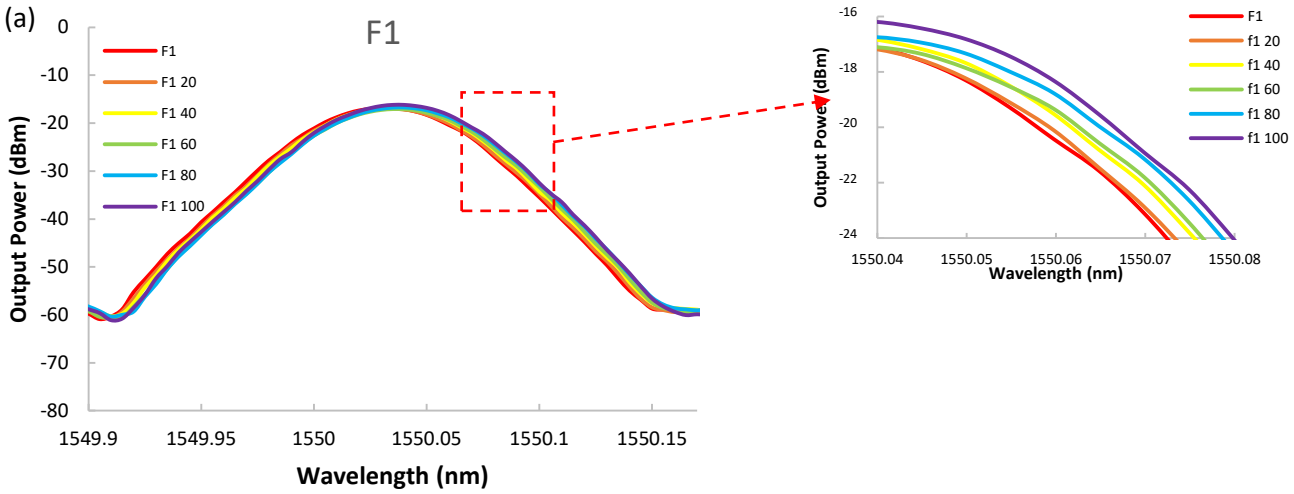
(a)
F1
F1
F1 20
F1 40
F1 60
F1 80
F1 100
Output Power (dBm)
Wavelength (nm)
f1 20
f1 40
f1 60
f1 80
f1 100

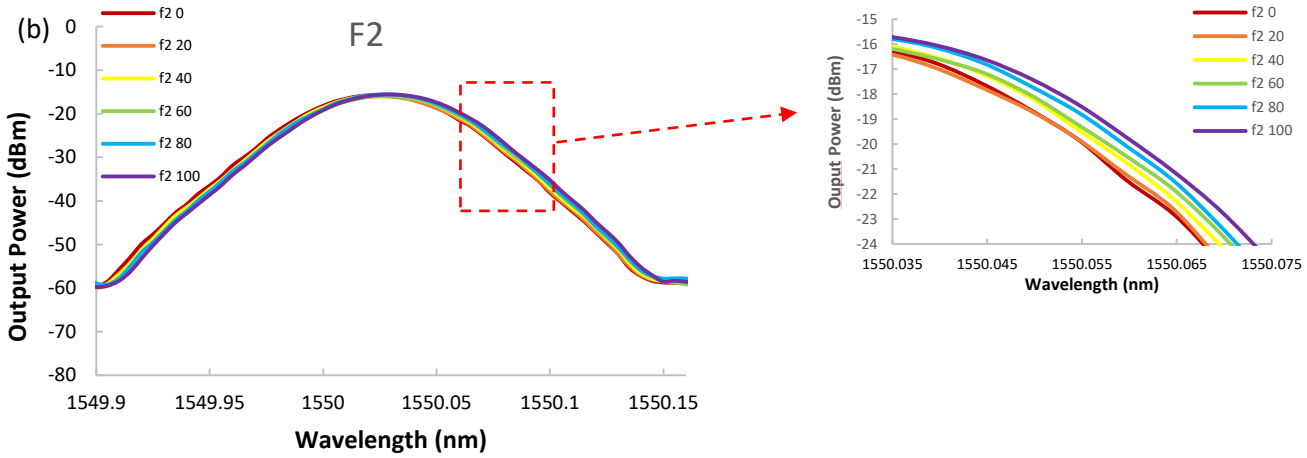
(b)
F2
f2 0
f2 20
f2 40
f2 60
f2 80
f2 100
Output Power (dBm)
Wavelength (nm)

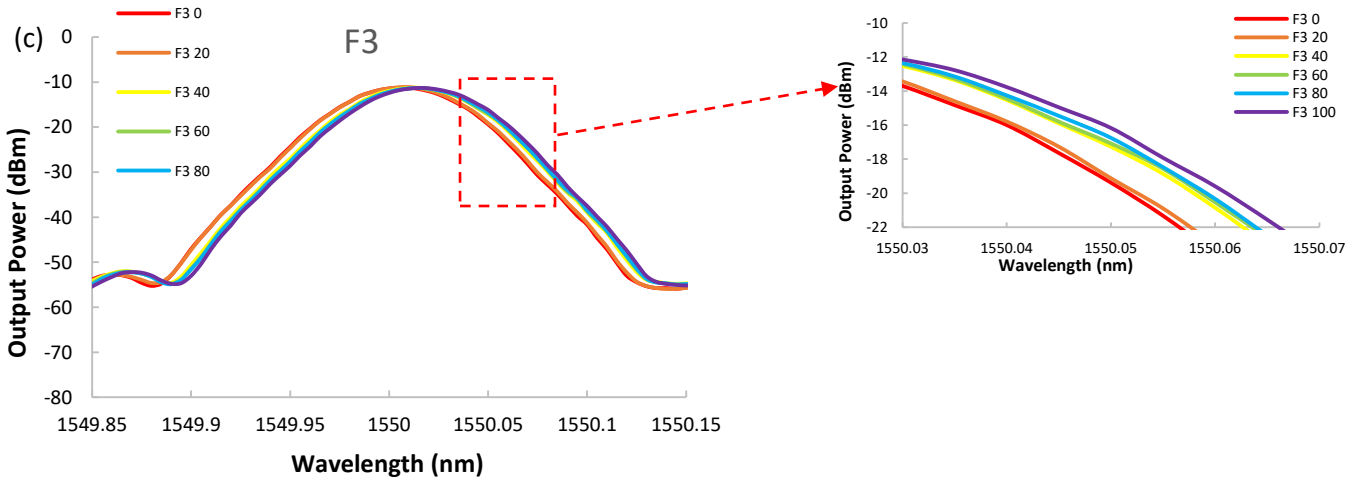
(c)
F3
F3 0
F3 20
F3 40
F3 60
F3 80
F3 100
Output Power (dBm)
Wavelength (nm)

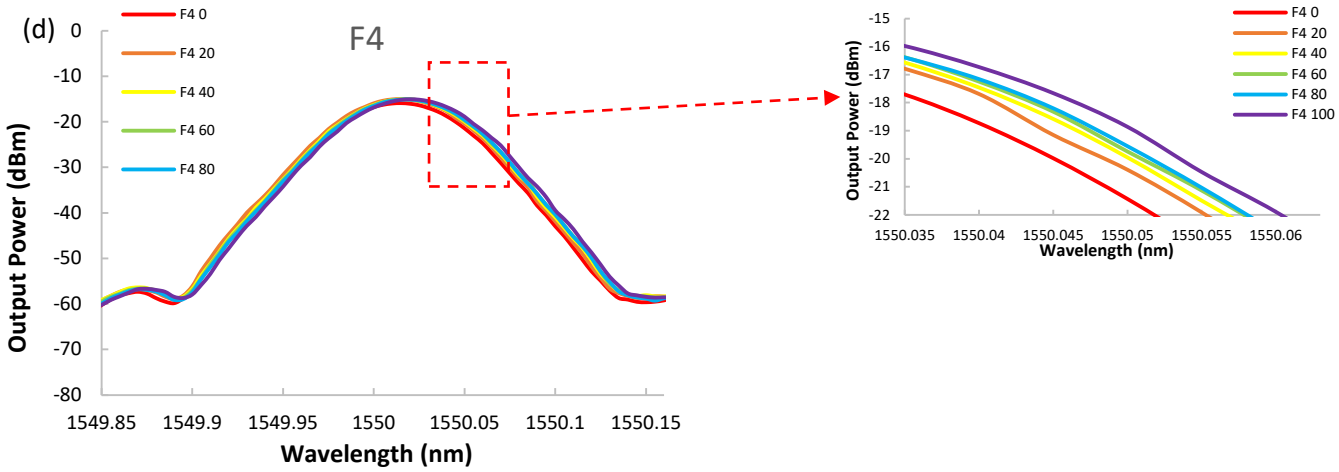

Fig. 5. Optical spectrum of ZnO-PVA-coated DSF at different IPA concentrations using (a) fiber 1, (b) fiber 2, (c) fiber 3, and (d) fiber 4 (colour online)

The decrease in sensing performance of fiber 1 is due to weak evanescent field interaction between light and liquid analytes on the DSF. Fiber 1 has lower sensing performance due to a low insertion loss, which limits the penetration of evanescent waves. By referring to Zainuddin et al., they found that DSF with no cladding exhibits stronger evanescent fields and higher sensitivity compared to fibers with a few microns of cladding [18]. This explains why fiber 1 exhibits lower sensing performance compared to the other DSFs. When the evanescent wave travels beyond the fiber with a very weak light-matter interaction, the probe will have a limited time to sense the RI changes in the surrounding environment, thus making the sensor less sensitive to the detected analyte. As observed in Fig. 6, the ZnO-PVA-coated DSFs exhibit a higher R^2 value compared to the uncoated DSF. The uncoated DSF has a linearity of 80% and sensitivity of 0.1166 nm/RIU. This confirms the improvement of the sensing probe with ZnO as a coating material.

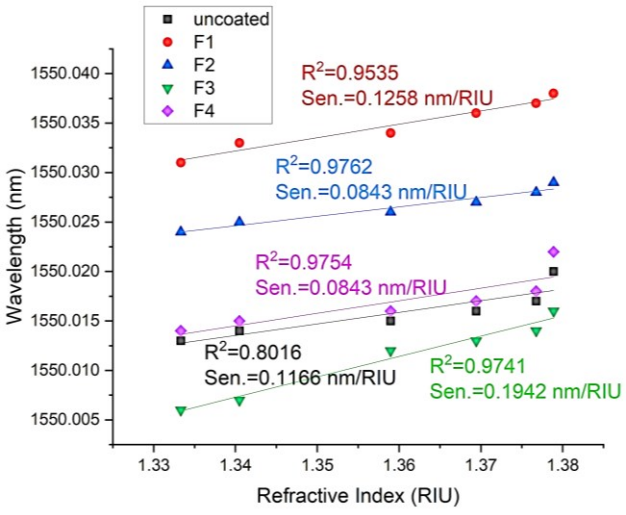

Fig. 6. Peak wavelength against the refractive index of IPA using ZnO-PVA-coated DSF with different polishing lengths (colour online)

Based on the parameters obtained from the experiment, fiber 3 has better sensing performance than the other three probes. Therefore, fiber 3 is said to have an optimum penetrating depth of the DSF structure. According to Cordaro et al. [19], fabricating the fiber beyond the cutoff penetrating depth will disrupt the light from traveling on the surface of DSF, while too-thin a polishing depth may produce a less sensitive sensing probe since the evanescent field is too weak. Therefore, it is significant to fabricate a D-shaped fiber probe with optimum polishing lengths and depth for effective RI sensing. We also verified the stability of the laser source with a patch cord by connecting it to the OSA. The results show a negligible alteration of the center wavelength when the tuneable ITU-grid DFB laser was set at 1550.00 nm. By repeating the experiment 10 times, the recorded center wavelength of the laser source is 1550.000 ± 0.002 nm. This indicates a reliable sensing setup for RI detection.

Table 1. The sensitivity, resolution, and linearity of F1, F2, F3, F4, and uncoated fiber as sensing probes for RI detection

Fiber	Sensitivity (nm/RIU)	Resolution (RIU)	Linearity (R^2)
F1	0.1258	2.10×10^{-2}	0.9535
F2	0.0843	2.22×10^{-2}	0.9762
F3	0.1942	2.05×10^{-2}	0.9741
F4	0.0843	3.36×10^{-2}	0.9754
uncoated	0.1166	2.13×10^{-2}	0.8016

5. Conclusion

In this study, we investigated the influence of polishing lengths of DSF on the sensitivity of DSF sensors. The fabricated DSF is polished using polishing

bits with diameters of 1, 2, 3, and 4 mm. By coating the surface of DSF with ZnO-PVA, we achieved the maximum sensitivity of 0.1942 nm/RIU within the refractive index range of 1.33-1.38, and a high resolution of 2.05×10^{-2} RIU, with a 3 mm bit. In addition, the proposed sensing probes own linearities within 0.95 to 0.97, suggesting a reliable sensing structure. Furthermore, our findings suggest that optimizing the polishing length significantly enhances the sensor's performance, making DSF a promising candidate for high-precision RI detection. Future work could explore the theoretical foundation behind polishing parameters and the real-world applications of these sensors in various industries.

Acknowledgements

This work was supported by a **Universiti Sains Malaysia, Short-Term Grant with Project No: R501-LR-RND002-0000000143-0000.**

The authors would also like to acknowledge the **Nano-Optoelectronics Research and Technology Laboratory (NOR Lab), School of Physics, Universiti Sains Malaysia,** for providing the equipment for material characterization. The authors would also like to thank ***Kumpulan Abex Sdn. Bhd. (KABEX)*** for providing an optical spectrum analyzer on loan for this project.

References

[1] A. I. Ferdous, M. N. R. Naim, K. S. Noor, D. Kundu, A. N. Z. Rashed, Cell Biochemistry and Biophysics **83**(1), 489 (2025).
[2] Y. Li, X. Li, Y. Liu, J. You, Y. Peng, H. Chen, Optical Fiber Technology **87**, 103891 (2024).
[3] G. Meng, N. Luan, H. He, F. Lei, J. Liu, Sensors **24**(13), 4335 (2024).
[4] A. A. S. Falah, W. R. Wong, G. A. Mahdiraji, F. R. M. Adikan, Optical Fiber Technology **74**, 103105 (2022).
[5] H. Qiu, W. Li, C. Zhu, J. Xu, J. Li, G. Bai, Journal of Optics **53**(3), 1897 (2024).
[6] M. Chekroun, M. Benali, I. Yahiaoui, M. Debab, M. Belmehdi, H. Tabet-Derraz, Optical Materials **132**, 112769 (2022).
[7] C. Soci, A. Zhang, B. Xiang, S. A. Dayeh, D. P. R. Aplin, J. Park, X. Y. Bao, Y. H. Lo, D. Wang, Nano Lett. **7**, 1003 (2007).
[8] M. Abdelkrim, M. Bedrouni, M. H. Bouslama, A. Ouerdane, B. Kharroubi, Journal of Alloys and Compounds **920**, 165703 (2022).
[9] A. Asture, V. Rawat, C. Srivastava, D. Vaya, Polymer Bulletin **80**(4), 3507 (2023).
[10] V. Kaushik, K. Bhardwaj, D. Kumar, M. Kumar, S. K. Sharma, Hybrid Advances **7**, 100295 (2024).
[11] Z. U. Paltusheva, Z. Ashikbayeva, D. Tosi, L. V. Gritsenko, Biosensors **12**(11), 1015 (2022).
[12] M. Chauhan, V. K. Singh, Current Applied Physics **50**, 38 (2023).
[13] Z. Yarar, M. Alyörük, H. Çekil, B. Özdemir, M. Özdemir, Physics of the Solid State **66**(4), 91 (2024).
[14] Q. Ren, Y. Ma, F. Liu, A. Zhang, K. Zhang, Journal of Optics **53**(4), 2891 (2024).
[15] L. Xiong, S. Duan, W. Wang, Y. Yao, H. Zhang, B. Liu, W. Lin, H. Liu, J. Wu, L. Lu, X. Zhang, Talanta **275**, 126168 (2024).
[16] Q. Zhang, W. Li, Q. Ren, J. Zheng, Q. Xie, X. Wang, Frontiers in Physics **10**, 1008784 (2022).
[17] H. Niu, Y. Li, Y. Zhang, Z. Yan, J. Kuang, G. An, Plasmonics **20**(1), 11 (2025).
[18] N. A. M. Zainuddin, M. M. Ariannejad, P. T. Arasu, S. W. Harun, R. Zakaria, Results in Physics **13**, 102255 (2019).
[19] M. Cordaro, D. L. Rode, T. Barry, R. R. Krchnavek, Journal of Lightwave Technology **12**(9), 1524 (2002).

*Corresponding author: afiqarif@usm.my